PCCP

ROYAL SOCIETY OF CHEMISTRY

PAPER

View Article Online
View Journal | View Issue

Cite this: *Phys. Chem. Chem. Phys.*, 2025, **27**, 7317

Structural evolution and electronic properties of boron sulfides $(B_2S_3)_n$ (n = 1–6): insights from DFT calculations†

Jingxin Hu, Lin Zhang and Zexing Cao *

Received 13th December 2024,
Accepted 11th March 2025

DOI: 10.1039/d4cp04699d

rsc.li/pccp

The low-energy isomers of boron sulfides $(B_2S_3)_n$ (n = 1–6) were constructed by using B_2S_3 as the building block, and their structure, stability, and reactivity toward small molecules have been explored by density functional theory (DFT) calculations. It is found that the low-energy isomers of $(B_2S_3)_n$ clusters are of rich bonding characteristics for their structural constituents, such as [S–B–S], $[B_2S_3]$, $[B_3S_3]$, [S], *etc.* The planar or non-planar B_2S_2 rings, as the basic structural units, are bridged together by the S atoms to form the most stable structures of $(B_2S_3)_n$ clusters with $n \geq 2$. These low-energy $(B_2S_3)_n$ clusters are predicted to be stable both structurally and electronically, and their boron centers show relatively high activity to the binding of small molecules NH_3 and CO, until all boron atoms are ligated by NH_3 or CO. The present results provide new insights into the structure and properties of $(B_2S_3)_n$ clusters, which are beneficial to the development of boron chemistry and the application of boron-based materials.

1. Introduction

Boron clusters and boron-containing compounds have attracted considerable attention due to their intriguing physical and chemical properties,[1–3] and numerous studies of theory and experiments have been conducted to explore the structural and bonding properties, spectroscopic characteristics, and chemical reactivity of boron clusters,[4–16] borophenes,[17–23] boron oxide clusters,[24–36] and so on. In particular, boron sulfide clusters and materials are of great interest because of their diverse structural features and bonding modes.[37–43]

In the 1960s and 1970s, White and Gilles *et al.* confirmed the existence of boron sulfides, including BS_2^+,[44] $B_2S_2^+$,[45,46] $B_2S_3^+$,[47,48] and so on, making a significant advancement in boosting the development of boron sulfide chemistry. The existing boron sulfide clusters can be categorized into three main types: proportional, sulfur-rich, and boron-rich boron sulfide clusters. In 2015, Li and co-workers presented a set of perfectly planar dicyclic $B_6S_6^{0/-/2-}$ clusters featuring a twin B_3S_2 five-membered ring as the core. It was found that the closed-shell $B_6S_6^{2-}$ exhibits a delocalized characteristic of 10π-electrons, closely analogous to the bonding pattern of the aromatic naphthalene.[49] Subsequently, Zheng and co-workers investigated the structural, electronic, and bonding properties of $BS^{0/-}$ and $BS_3^{0/-}$ by combining experimental and theoretical methods.[50] The results reveal that the ground state of BS_3^- has a planar structure with C_{2v} symmetry, whereas BS_3 presents an S–B–S–S bending structure. Recently, Chen and co-workers explored the structural evolution of $B_nS_2^{0/-}$ (n = 2–13) clusters through the DFT calculations combined with particle swarm optimization algorithm software, and the predicted global minima for these clusters suggest a conformational evolution from a linear-chain structure to planar or quasi-planar ones.[51] Obviously, while the above theoretical and experimental studies show that boron sulfide clusters exhibit very rich chemical bonding modes, depending on the B/S atomic ratio and the charged state, our understanding of B_2S_3-type clusters remains insufficient.

Notably, B_2O_3-type clusters were proved to play a crucial role in boron chemistry and oxidative dehydrogenation of propane.[52–57] In 2013, Li and Cheng theoretically studied the structure evolution and electronic properties of $(B_2O_3)_n$ (n = 1–6) clusters, and found that the global minima structures of these clusters are planar up to n = 3, and cages at n = 4–6.[58] Given the similarity in the valence electron configurations of sulfur and oxygen atoms, $(B_2S_3)_n$ and $(B_2O_3)_n$ may exhibit similar structural and electronic features. This also implies that B_2S_3-type clusters could display analogous chemical properties and stability, making them ideal candidates for organic catalysis and materials science.

Recently, B_2S_3-type two-dimensional (2D) materials were predicted to be promising catalysts for splitting water[59,60] and suppressing the

State Key Laboratory of Physical Chemistry of Solid Surfaces and Fujian Provincial Key Laboratory of Theoretical and Computational Chemistry, College of Chemistry and Chemical Engineering, Xiamen University, Xiamen, China 361005.
E-mail: zxcao@xmu.edu.cn

† Electronic supplementary information (ESI) available: Functional testing; low-energy structures of charged clusters; AdNDP analysis; optimized structures of studied molecular compounds; key interaction analysis between $[B_2S_3]$ with NH_3 and CO molecules; absolute free energies and electronic energies; and Cartesian coordinates. See DOI: https://doi.org/10.1039/d4cp04699d

shuttle effect in lithium–sulfur batteries.[61] However, our knowledge of B_2S_3-type clusters in terms of their structural evolution and chemical properties is still very limited. Further investigation into the growth of B_2S_3-type clusters could lead to the development of more stable and efficient materials for these applications.

Under this background, B_2S_3 has been chosen as a fundamental structural unit to search for the stable structures of a series of $(B_2S_3)_n$ (n = 1–6) clusters by using the artificial bee colony algorithm.[62,63] Subsequent DFT calculations were used to determine the structural and electronic properties of the corresponding low-energy structures of $(B_2S_3)_n$. Additionally, the interaction of selected clusters with small molecules was discussed to explore their potential applications in small molecule activation and capture. The present work aims to further understand the structures, properties, and potential applications of boron sulfide clusters, and to provide a theoretical basis for the development of 2D boron-based materials.

2. Computational details

The low-energy structures of the studied $(B_2S_3)_n$ clusters are predicted by using the artificial bee colony algorithm, implemented in the ABCluster software for the global optimization of chemical clusters.[62,63] The initial configurations, ranging from 1000 to 80 000 depending on the number of atoms in the studied clusters, are auto-generated and pre-optimized by the semiempirical PM6 and GFN2-*x*TB method with ABCluster.[64–67] Then 80 searched structures with relatively low energy for the studied clusters are selected and fully optimized with the more accurate DFT method at the M06-2X-D3[68,69]/6-31G(d,p)[70,71] level of theory, implemented in the Gaussian 16 package.[72] The final energy ranking of low-energy structures is obtained through a combination of PM6 and GFN2-*x*TB methods, effectively reducing the risk of missing important structures. All the optimized cluster structures underwent harmonic vibrational analysis at the same level, confirming that all the related species are stable without imaginary frequency. In addition, the composite quantum chemical method G4(MP2)-6X[73] is adopted to evaluate the reliability of the M06-2X-D3/6-31G(d,p) level. Mayer bond order,[74] adaptive natural density partitioning (AdNDP),[75] and orbital composition analyses are performed by the Multiwfn program.[76] Geometric structures and molecular orbitals were visualized by using the CYLview,[77] IboView,[78] and VMD programs.[79]

3. Results and discussion

Low-energy structures

Based on the results searched by using ABCluster, some low-energy structures of $(B_2S_3)_n$ (n = 1–6) clusters have been identified. Prior to investigating the structural and electronic properties of these clusters in detail, a comparative analysis was conducted on the equilibrium structures and relative energy order of selected low-energy clusters evaluated by both the M06-2X-D3/6-31G(d,p) and G4(MP2)-6X methods, and there are no qualitative differences between the results obtained by the two methods, thereby confirming that the M06-2X-D3/6-31G(d,p) approach is capable of accurately evaluating the structures and properties of the studied boron-based clusters (see more details in Fig. S1–S6, ESI†). Herein, the following discussion mainly focuses on clusters with relative Gibbs free energies below 30.0 kcal mol^{-1} at the M06-2X-D3/6-31G(d,p) level, as well as the isomers similar to the most stable $(B_2O_3)_n$ cluster structures in previous studies.[25,58]

As shown in Fig. 1, the most stable isomer **I** of the B_2S_3 cluster exhibits a V-shaped structure with alternating bonding between B and S atoms. In contrast, isomers **II** (T-shaped) and **III** (Y-shaped) with a B–B motif are less stable than **I** by 22.5 and 29.0 kcal mol^{-1}, respectively. For the B_4S_6 cluster, the most stable isomer **I** features a B_2S_2 rhombic core with two linear [S–B–S] arms in a *trans*-configuration, and its corresponding cis-configuration **II** is almost isoenergetic with **I**. The isomer **III** of B_4S_6 with two non-planar B_2S_2 units linked by S atoms is lying at 12.8 kcal mol^{-1} above **I**. Notably, both isomers **IV** and **V** without the B_2S_2 moiety, with the boron-centered structure connecting three linear [S–B–S] motifs, are higher in energy than **I** by 19.4 and 22.3 kcal mol^{-1}, respectively. For relatively large clusters of B_6S_9, B_8S_{12}, $B_{10}S_{15}$, and $B_{12}S_{18}$, their most stable isomers generally consist of several planar or non-planar B_2S_2 rings as the main structural units, connected by S atoms to form a closed structure. Obviously, their higher-energy structures tend to feature six-membered $[B_3S_3]$ rings or linear [S–B–S] structural units. Overall, the low-energy isomers of $(B_2S_3)_n$ clusters with n = 1 and 2 mainly exhibit a planar configuration, whereas a non-planar or cage configuration is adopted for the large-sized clusters with n = 3–6.

Interestingly, it was found that the most stable isomers of B_2S_3 and B_4S_6 have the same configuration as that of the corresponding B_2O_3 and B_4O_6 clusters.[25,58] Conversely, for relatively large clusters such as B_6S_9, B_8S_{12}, $B_{10}S_{15}$, and $B_{12}S_{18}$, the isomers with structures similar to the corresponding boron oxide clusters are less stable than the most stable species by more than 20.0 kcal mol^{-1}. For instance, **VI** in B_6S_9, **V** in B_8S_{12}, **III** in $B_{10}S_{15}$, and **II** in $B_{12}S_{18}$ are higher in energy than their respective most stable isomers by 45.8, 63.0, 47.8, and 23.9 kcal mol^{-1}, respectively. Presumably, there may be significant differences in structural and electronic properties between the boron sulfide $(B_2S_3)_n$ and boron oxide $(B_2O_3)_n$ clusters.

Fig. 2a presents key bond lengths, Mayer bond orders, and bond angles for the most stable isomers of $(B_2S_3)_n$ (n = 1–6) clusters. For planar B_2S_3 and B_4S_6 featuring linear [S–B–S] arms, the bonding between the terminal S and B atoms is intermediate between a double and a triple bond, with a Mayer bond order of 2.453 and bond lengths around 1.605 Å. For relatively large clusters, their most stable isomers are composed of planar or non-planar B_2S_2 cyclic structures bonded together by the sulfur atom, such as B_4S_6, B_6S_9, B_8S_{12}, $B_{10}S_{15}$, and $B_{12}S_{18}$, where the B–S single bonds vary from 1.809 to 1.832 Å. Furthermore, the natural adaptive orbital (NAdO) analyses are performed to describe the distribution, character, and intensity of the chemical bonding.[80,81] The NAdO analysis reveals that the terminal B–S bond in B_4S_6 is characterized by three major NAdOs, one σ-type (0.914) and two π-type (0.621 and 0.601) bonding categories, and the occupancy sum of σ and π NAdOs is 2.116, indicating that the terminal B–S bond is between double and triple bonds, as shown by the Mayer bond order (2.453) analysis.

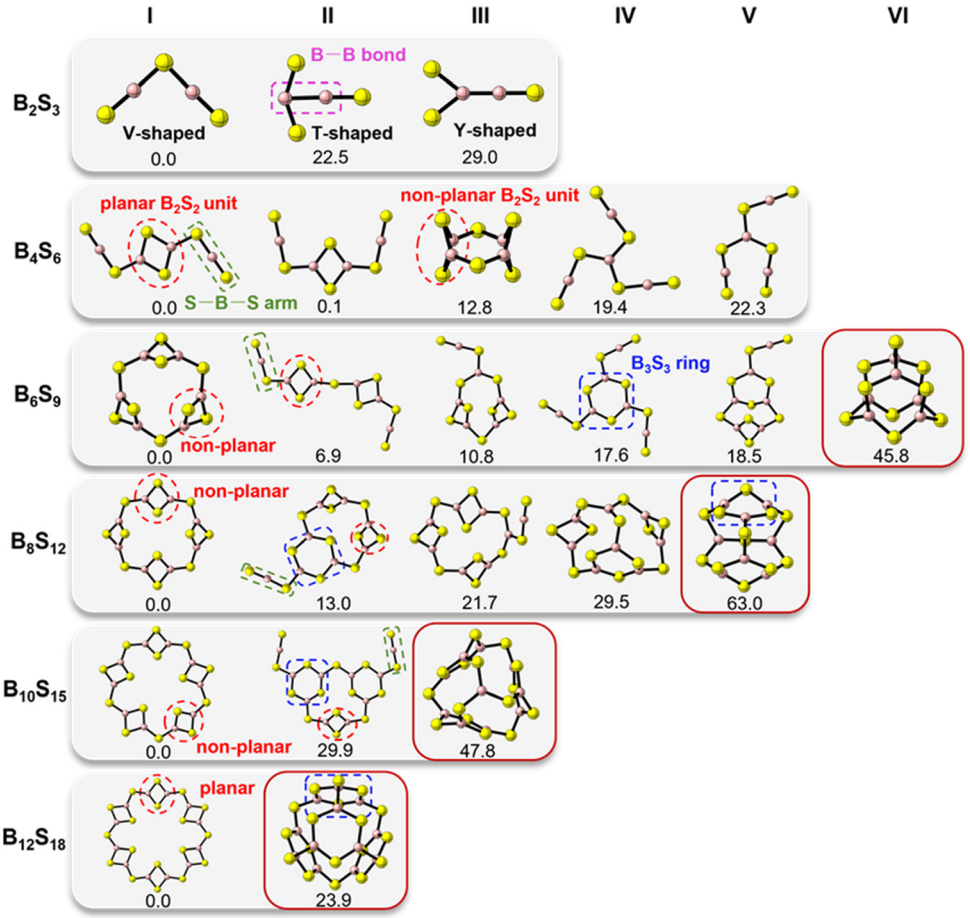

Fig. 1 The optimized low-energy structures and relative free energies (in kcal mol^{-1}) of the studied boron sulfide clusters, where B and S atoms are in pink and yellow, respectively.

Bonding and stability

In order to gain a deeper understanding of the bonding properties of the most stable isomer of the studied clusters, the adaptive natural density partitioning (AdNDP) method is employed to describe the key delocalized orbitals and bonding characteristics, as depicted in Fig. 3 and Fig. S7 (ESI†). For B_2S_3 in Fig. 3a, there are two lone pairs (LPs) of electrons on the S atoms with the occupied number (ON) of 1.96 |e|, four two-center two-electron (2c–2e) σ-bonds (ON = 1.99–2.00 |e|) from the inner B—S bond, four 2c–2e π-bonds (ON = 1.98–2.00 |e|) from the terminal B—S bond, and one 3c–2e π-bond (ON = 1.96–1.97 |e|). For B_4S_6 in Fig. 3b, there are four lone pairs of electrons mainly originating from the S atoms, ten 2c–2e σ bonds, four 2c–2e π bonds, two 3c–2e π bonds, one 4c–2e π bond, and one 2c–2e π* bond. It was found that the cyclic B_2S_2 structure is characterized by σ, π, and π* bonds. Note that the large-sized B_6S_9, B_8S_{12}, $B_{10}S_{15}$, and $B_{12}S_{18}$ clusters have similar bonding characteristics, mainly including LPs on the S atoms, 2c–2e σ-bonds for the B—S single bonds, delocalized 3c–2e π-bonds contributed by the B—S—B units, and 4c–2e π-bonds and 2c–2e π*-bonds from the planar or non-planar B_2S_2 rings. Overall, the AdNDP analysis further deepens our understanding of the structures and bonding properties of the selected clusters.

Additionally, the bonding strength between $(B_2S_3)_n$ clusters and the B_2S_3 monolayer[52] are compared under the same theoretical level (see more details in Table S3, ESI†). The results show that the bonding energy of the B—S bonds in $(B_2S_3)_n$ clusters is generally stronger than that of the B_2S_3 monolayer (except B_6S_9 cluster). The B_6S_9 cluster has a lower bonding energy than the B_2S_3 monolayer, indicating its lower stability.

The key frontier molecular orbitals and the corresponding energy levels of the most stable clusters are shown in Fig. 4. It was found that the HOMO of B_2S_3 originates from the terminal B—S π bonding and the non-bonding 3p orbital of the *meso* S atoms, whereas the LUMO is characterized by the B—S antibonding (π*). Similarly, the HOMO of B_4S_6 is derived from the terminal B—S π bonding and the 3p orbitals of the connected S atoms, and its LUMO is mainly contributed by the S atoms of the B_2S_2 moiety. For the large-sized clusters, such as B_6S_9, B_8S_{12}, $B_{10}S_{15}$, and $B_{12}S_{18}$, their HOMOs and LUMOs are primarily composed of the 3p orbitals of S atoms and the 2p orbitals of B atoms, respectively. As shown in Fig. 4b, these boron sulfide clusters generally have relatively large HOMO–LUMO gaps (E_{GAP} = 4.36–5.14 eV), indicating that all the studied $(B_2S_3)_n$ (n = 1–6) clusters may possess highly stable electronic structures. As the number of B_2S_3 basic units increases, the E_{GAP} value decreases first and then maintains at about 4.4 eV.

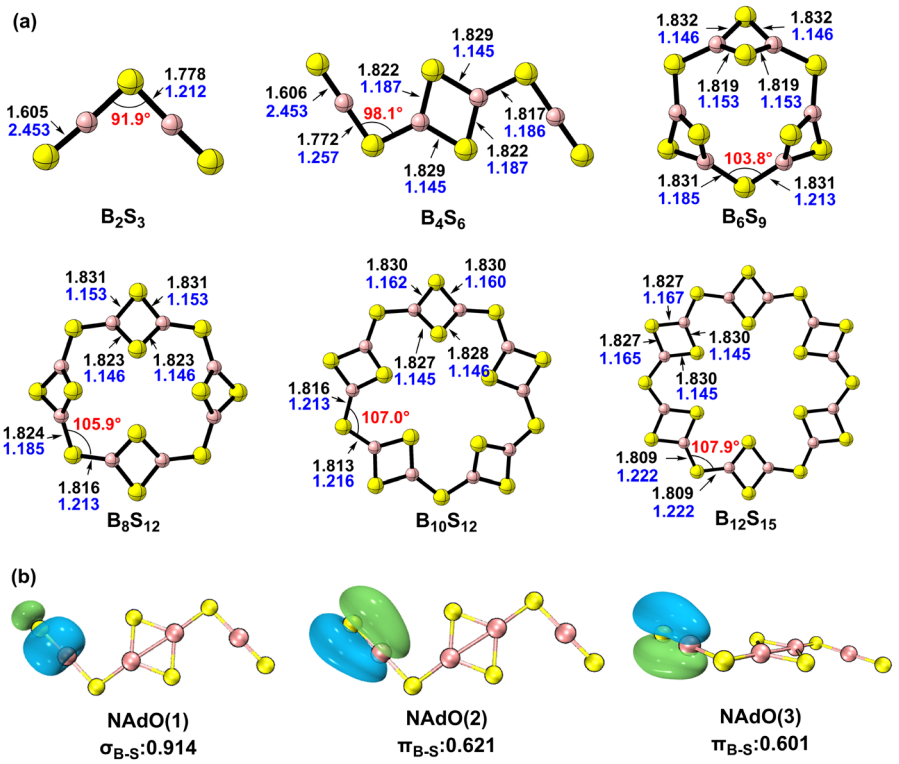

Fig. 2 (a) The optimized global minimum configurations of the studied $(B_2S_3)_n$ clusters, where the key bond lengths (Å), Mayer bond orders, and bond angles (°) are given in black, blue, and red, respectively. (b) The NAdO analysis on the bonding modes of B_4S_6 is given, where B and S atoms are in pink and yellow, respectively.

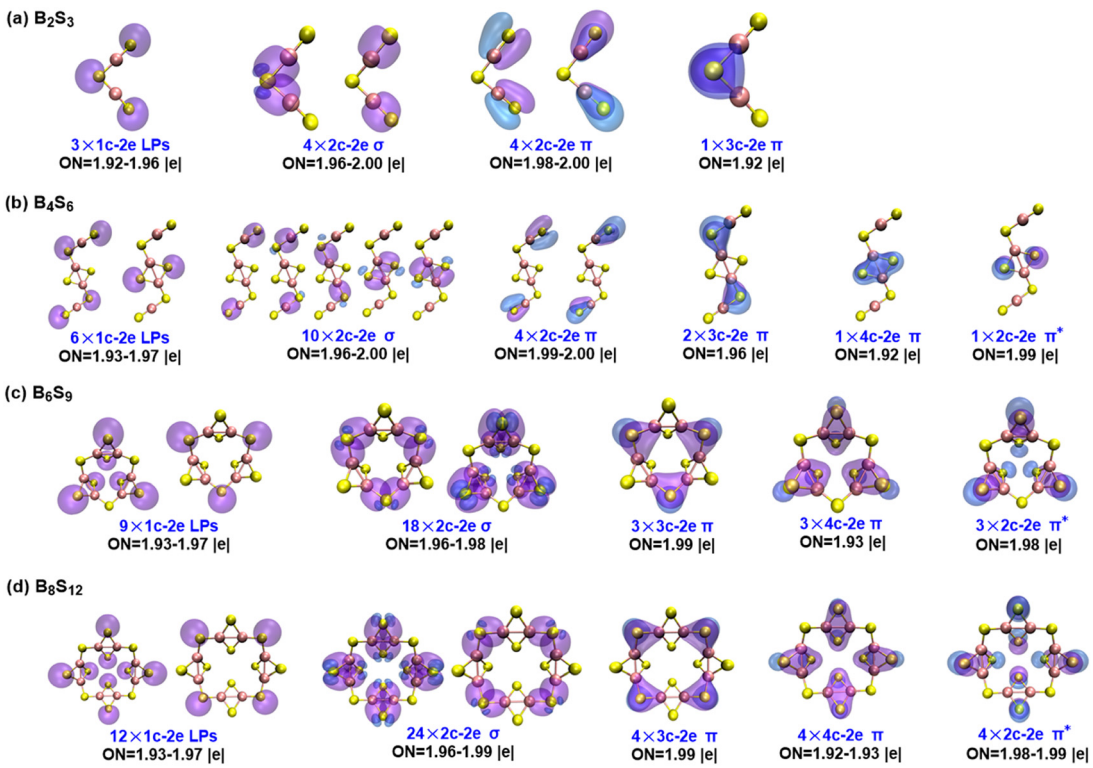

Fig. 3 AdNDP delocalized bonding patterns and the corresponding occupied numbers for (a) B_2S_3, (b) B_4S_6, (c) B_6S_9, and (d) B_8S_{12}. The color of atoms: B-pink; S-yellow.

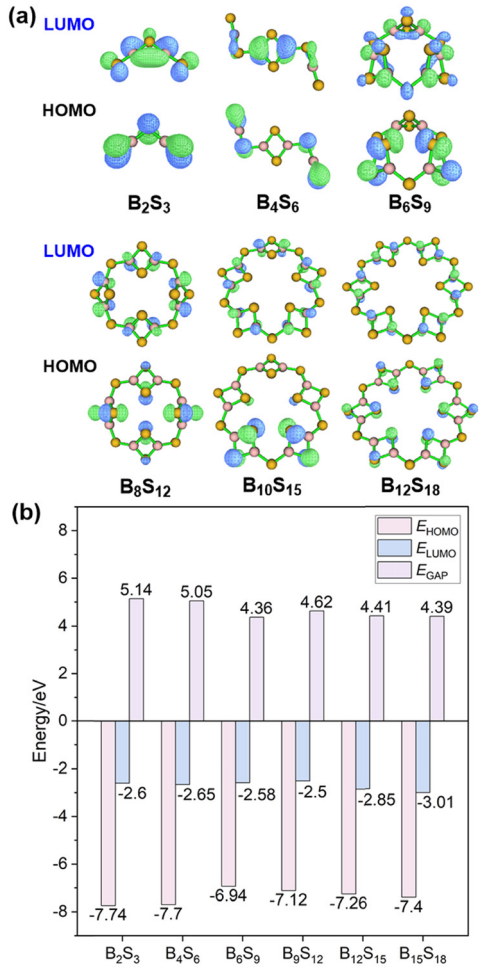

Fig. 4 (a) The key molecular orbitals (isosurface = 0.05) and (b) the corresponding energy levels (in eV) of the studied $(B_2S_3)_n$ clusters.

In order to understand the electronic gain and loss characteristics as well as the relative stability of these studied boron sulfide clusters, their adiabatic/vertical electron affinities (EA_a and EA_v) and adiabatic/vertical ionization potentials (IP_a and IP_v), average binding energies (E_b), and second-order energy difference (Δ^2E) were calculated as follows:

$$EA_a = E^0_{therm} - E^{-1}_{therm}$$

$$EA_v = E^0 - E^{-1}$$

$$IP_a = E^1_{therm} - E^0_{therm}$$

$$IP_v = E^1 - E^0$$

$$E_{therm} = E_{elec} + E_{corr}$$

$$E_b([B_2S_3]_n) = \frac{2nE(B) + 3nE(S) - E([B_2S_3]_n)}{5n}$$

$$\Delta^2E([B_2S_3]_n) = E([B_2S_3]_{n-1}) + E([B_2S_3]_{n+1}) - 2E([B_2S_3]_n)$$

Table 1 Calculated EA_a, EA_v, IP_a, IP_v, E_b, and Δ^2E of the studied clusters at the B3LYP/def2-TZVP level[a]

Cluster	EA_a (eV)	EA_v (eV)	IP_a (eV)	IP_v (eV)	E_b (eV)	Δ^2E
B_2S_3	1.79	0.69	9.60	9.73	0.1860	—
B_4S_6	1.63	1.17	9.13	9.23	0.1922	0.2720
B_6S_9	1.77	1.18	8.08	8.51	0.1936	−0.9400
B_8S_{12}	1.87	1.30	8.26	8.42	0.1961	0.2335
$B_{10}S_{15}$	2.00	1.77	8.50	8.45	0.1972	0.2345
$B_{12}S_{18}$	1.25	2.03	8.51	8.42	0.1976	—

[a] Adiabatic electron affinities EA_a, vertical electron affinities EA_v, adiabatic ionization potentials IP_a, vertical ionization potentials IP_v, average binding energies E_b, and second-order energy difference Δ^2E.

where E^0, E^1, and E^{-1} denote the electronic energies of the neutral $(B_2S_3)_n$ clusters, and their negative and positive ions with ±1 charge, respectively, and E^0_{therm}, E^1_{therm}, and E^{-1}_{therm} denote the sum of the corresponding electronic energies (E_{elec}) and thermally corrected electronic energies (E_{corr}) for the ground states of the neutral $(B_2S_3)_n$ clusters and their charged states. To obtain the adiabatic quantities of EA and IP, we have conducted independent unbiased searches for the charged clusters, and the corresponding low-energy structures are presented in Fig. S7–S18 (ESI†). It should be note that global minima are partly different for neutral and charged clusters.

As shown in Table 1, as the cluster size increases, the EA_v values gradually increase overall, while the IP_a and IP_v values correspondingly decrease first and then remain less varied. Additionally, the EA_a value of $B_{12}S_{18}$ is exceptionally low at 1.25 eV, primarily attributed to significant structural reorganization upon the formation of the anion cluster $B_{12}S_{18}^-$ (see more details in Fig. S16, ESI†). Notably, the relatively low EA_a and EA_v values suggest a diminished capability of the molecule to accommodate additional electrons, whereas the relatively large IP_a and IP_v values indicate that the corresponding clusters are highly stable in their neutral state. These observations collectively underscore the high chemical stability of the studied boron sulfide clusters. Note that the evaluated EAs and IPs are closely correlated with the frontier molecular orbital properties of the studied molecules. There is a sharp drop in IPs from B_4S_6 to B_6S_9, which can be ascribed to the transition of the HOMO composition from predominant π orbitals associated with B–S bonds to the 3p orbitals of S atoms.

The slightly increasing E_b suggests that the stability of $(B_2S_3)_n$ (n = 1–6) clusters gradually enhances with the increase in cluster size. Furthermore, the second-order differences (Δ^2E) reveal a different perspective on stability. Although most isomers have positive Δ^2E values, B_6S_9 stands out with a significantly negative Δ^2E value of −0.9400, suggesting a higher reactivity structurally, compared to the other clusters. Overall, these studied clusters show relatively high stability both structurally and electronically.

Infrared spectroscopy

To facilitate future identification of B_2S_3-type clusters, the predicted infrared spectra of the selected clusters are collected in Fig. 5. Note that the infrared spectrum of B_2S_3 shows two

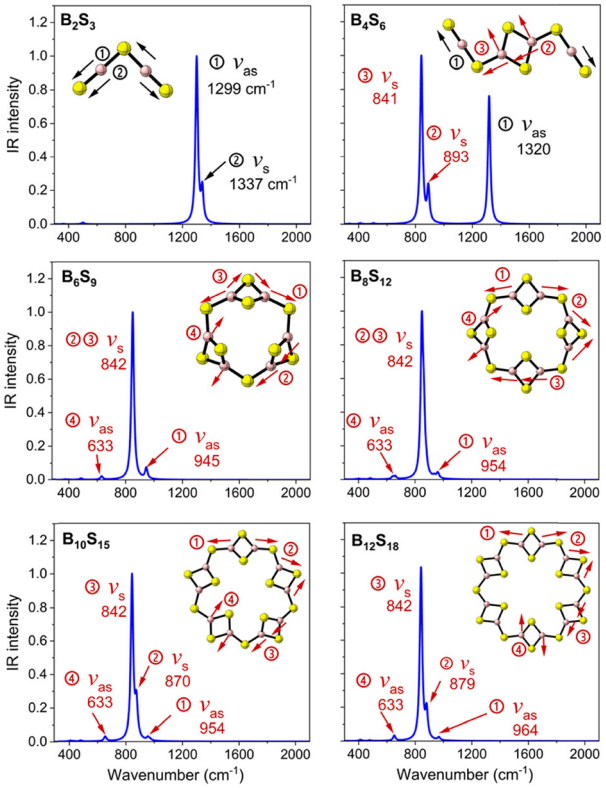

Fig. 5 Predicted infrared spectra of the studied $(B_2S_3)_n$ clusters at the B3LYP/def2-TZVP level of theory.

notable absorption bands, where the stronger peak at 1299 cm^{-1} and the weaker one at 1337 cm^{-1} arise from the asymmetric and symmetric stretching vibrations of both [S–B–S] units, respectively. The infrared spectrum of B_4S_6 displays three key vibrational absorption bands, where the adsorptions at 841 and 1320 cm^{-1} are attributed to the symmetric and asymmetric stretching vibrations of the [S–B–S] unit, respectively, whereas the peak at 893 cm^{-1} arises from the symmetric deformation of the B_2S_2 ring along the direction of B atoms. Additionally, the infrared spectra of B_6S_9, B_8S_{12}, $B_{10}S_{15}$, and $B_{12}S_{18}$ share a common pattern due to their primary cyclic B_2S_2 structural units, and their main vibrational peaks all located at 842 cm^{-1}, which are attributed to the breathing vibrations of the B_2S_2 unit. Overall, the infrared spectral characteristics are closely tied to the core structural units of each cluster, which provide a theoretical basis to identify and distinguish the structure of B_2S_3-type clusters.

Interactions of $(B_2S_3)_n$ with small molecules

Due to the electron-deficient nature of boron, boron clusters and their derivatives often exhibit chemical reactivity toward small molecules.[82–86] Herein, it was found that the selected boron sulfide clusters can interact with small molecules, particularly NH_3 and CO, and the main binding modes were elucidated, based on DFT calculations. The binding energies (ΔE) were determined as follows:

$$\Delta E = E_{B_2S_3X_m} - (E_{B_2S_3} + m \times E_X)$$

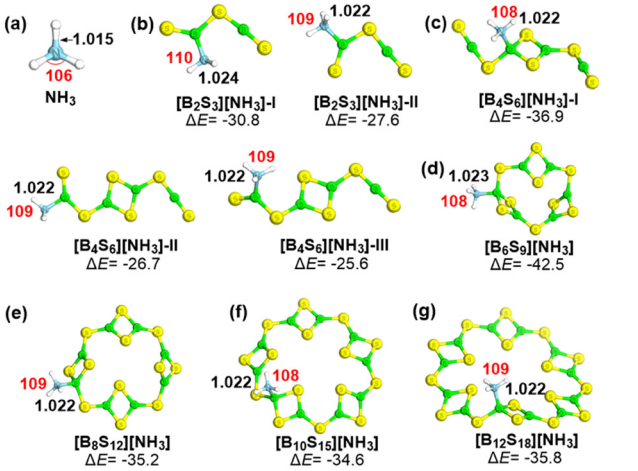

Fig. 6 The optimized structures and the relative energies (ΔE, in kcal mol^{-1}) of the NH_3 molecule (a) and studied complexes $[B_2S_3]_n[NH_3]$ (b–g), taking the energy sum of individual components as the reference. Key N–H bond lengths (Å) and H–N–H angles (°) are given in black and red, respectively. The color of atoms: S-yellow; B-green; N-blue; H-white.

in which X and m represent the involved small molecules and their corresponding numbers, respectively.

As shown in Fig. 6, main interaction modes between $(B_2S_3)_n$ (n = 1–6) clusters and NH_3 are explored. Note that the complexation between NH_3 and the B atom of $(B_2S_3)_n$ is actually a Lewis acid–base interaction. As shown in Fig. 6b, the complex of NH_3 and B_2S_3 exhibits two configurations, arising from the nucleophilic attack of NH_3 on the B site from both inside and outside the V-shaped structure, while the overall structure remains planar. Energetically, $[B_2S_3][NH_3]$-I is a more stable configuration. According to the relative energies of various binding modes between B_4S_6 and NH_3 in Fig. 6c, it was found that NH_3 more readily binds to the cyclic B_2S_2 moiety rather than the linear [S–B–S] unit, with a difference in ΔE exceeding 10.0 kcal mol^{-1}. The binding interaction of NH_3 with the global minimum structure of clusters B_6S_9, B_8S_{12}, $B_{10}S_{15}$, and $B_{12}S_{18}$, forms a similar stable configuration, with the B atom in the B_2S_2 moiety as the main active site. Notably, the N–H bond (1.015 Å) and the H–N–H bond angle (106°) of NH_3 increase to some extent, upon binding to the selected clusters, as shown in Fig. 6. Overall, the studied clusters can stably adsorb NH_3 molecules through the Lewis acidity of their B atoms, which may be used for capture and separation of small molecules.

Subsequently, the interactions of $(B_2S_3)_n$ (n = 1–6) clusters with carbon monoxide (CO) are further explored, as depicted in Fig. 7. We note that the bond length of the CO adsorbed at the B atom of the [S–B–S] unit is almost unchanged (1.132 ~ 1.134 Å), compared to the free molecule, but the CO molecule bound to the B atom of the cyclic B_2S_2 moiety has a shortened C≡O bond with the bond length of about 1.27 Å, suggesting that the formation of a B–CO dative bond is beneficial to the dispersion of excess electrons on the carbon atom and thus further enhances the CO bonding interaction. The predicted binding energies (ΔE) range from −13.3 to −4.7 kcal mol^{-1}, where the B_6S_9 cluster has the strongest interaction toward CO among these clusters considered here.

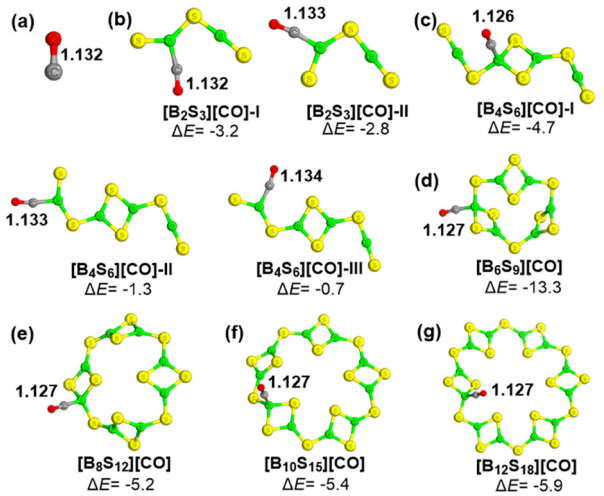

Fig. 7 The optimized structures of the CO molecule (a) and studied complexes $[B_2S_3]_n$[CO] (b–g), and their corresponding CO binding energies (ΔE, in kcal mol^{-1}), where key C–O bond lengths (Å) are given in black. The color of atoms: S-yellow; B-green; C-gray; O-red.

As Fig. 6 and 7 show, B_6S_9 has the strongest binding interaction with both NH_3 and CO molecules among the boron sulfide clusters here. In addition, we investigated the interactions of $(B_2S_3)_n$ clusters with multiple NH_3 or CO molecules, and the optimized structures and corresponding bind energies of these complexes $[B_2S_3]_n[NH_3]_m$ and $[B_2S_3]_n[CO]_m$, are presented in Fig. S8 and S9 (ESI†). Overall, all B atoms of these boron sulfide clusters can bind these small molecules until the boron sites are saturated.

Overall, the present results suggest that B_2S_3-type clusters exhibit potential applications in organic catalysis and materials engineering, specifically reflected in the following aspects: (a) the strong Lewis acidity of electron-deficient boron centers may facilitate the catalytic activation of small molecules, analogous to established B–N catalytic systems;[87,88] (b) the structural stability and delocalized electron characteristics observed in these clusters provide design principles for developing novel 2D boron–sulfide materials with graphene-like architectures; (c) the bonding energy of the B–S bonds in $(B_2S_3)_n$ clusters is generally stronger than that in the reported B_2S_3 monolayer,[52] suggesting that the predicted clusters may offer broader application prospects compared to the B_2S_3 monolayer materials due to their enhanced stability.

4. Conclusions

Herein, DFT calculations combined with the artificial bee colony algorithm were used to investigate the structural evolution, bonding and reactivity of $(B_2S_3)_n$ clusters. The computational results indicate that the low-energy isomers of these boron sulfides have different structural features as the number of B_2S_3 basic units increases. In particular, the global minimum structures of B_2S_3 and B_4S_6 present a planar configuration, while for the larger-sized clusters of $(B_2S_3)_n$ with n = 3–6, their global minimum configurations are mainly non-planar or cage-like structures. Overall, the linear [S–B–S] and cyclic B_2S_2 structures are the primary constituent units of these clusters. These structural features differ from those observed in $(B_2O_3)_n$-type clusters to some extent. The most stable structures of relatively large $(B_2S_3)_n$ clusters are generally assembled by the cyclic B_2S_2 motifs through S atoms as the linker, and the multiple bonding interactions, including 2c-2e σ and π bonds, 3c-2e and 4c-2e π bonds, lone pairs, *etc.*, are responsible for their relatively high stability both structurally and electronically. These boron sulfides show high activity toward the capture of small molecules NH_3 and CO. The computational findings suggest that these $(B_2S_3)_n$ clusters are promising for the development of boron-based functional materials.

Data availability

The data supporting this article have been included as part of the ESI.†

Conflicts of interest

The authors declare that the research was conducted in the absence of any commercial or financial relationships that could be construed as a potential conflict of interest.

Acknowledgements

This work is supported by the National Natural Science Foundation of China (22373078 and 21933009).

References

1 R. Núñez, M. Tarrés, A. Ferrer-Ugalde, F. F. de Biani and F. Teixidor, *Chem. Rev.*, 2016, **116**, 14307–14378.
2 V. Avdeeva, E. Malinina and N. Kuznetsov, *Coordin. Chem. Rev.*, 2022, **469**, 214636.
3 R. J. Grams, W. L. Santos, I. R. Scorei, A. Abad-García, C. A. Rosenblum, A. Bita, H. Cerecetto, C. Viñas and M. A. Soriano-Ursúa, *Chem. Rev.*, 2024, **124**, 2441–2511.
4 S. Pan, J. Barroso, S. Jalife, T. Heine, K. R. Asmis and G. Merino, *Acc. Chem. Res.*, 2019, **52**, 2732–2744.
5 N. G. Szwacki, A. Sadrzadeh and B. I. Yakobson, *Phys. Rev. Lett.*, 2007, **98**, 166804.
6 A. Ray, I. Howard and K. Kanal, *Phys. Rev. B: Condens. Matter Mater. Phys.*, 1992, **45**, 14247–14255.
7 A. P. Sergeeva, Z. A. Piazza, C. Romanescu, W. L. Li, A. I. Boldyrev and L. S. Wang, *J. Am. Chem. Soc.*, 2012, **134**, 18065–18073.
8 S. Li, Z. Zhang, Z. Long, G. Sun and S. Qin, *Sci. Rep.*, 2016, **6**, 25020.
9 A. P. Sergeeva, D. Y. Zubarev, H. J. Zhai, A. I. Boldyrev and L. S. Wang, *J. Am. Chem. Soc.*, 2008, **130**, 7244–7246.
10 J. I. Aihara, H. Kanno and T. Ishida, *J. Am. Chem. Soc.*, 2005, **127**, 13324–13330.
11 A. P. Sergeeva, I. A. Popov, Z. A. Piazza, W. L. Li, C. Romanescu, L. S. Wang and A. I. Boldyrev, *Acc. Chem. Res.*, 2014, **47**, 1349–1358.

12 I. Boustani, *Chem. Phys. Lett.*, 1995, **240**, 135–140.
13 I. Boustani, *Phys. Rev. B: Condens. Matter Mater. Phys.*, 1997, **55**, 16426–16438.
14 T. Jian, X. Chen, S. D. Li, A. I. Boldyrev, J. Li and L. S. Wang, *Chem. Soc. Rev.*, 2019, **48**, 3550–3591.
15 H. Kato, K. Yamashita and K. Morokuma, *Chem. Phys. Lett.*, 1992, **190**, 361–366.
16 W. L. Li, Y. F. Zhao, H. S. Hu, J. Li and L. S. Wang, *Angew. Chem., Int. Ed.*, 2014, **53**, 5540–5545.
17 W. L. Li, X. Chen, T. Jian, T. T. Chen, J. Li and L. S. Wang, *Nat. Rev. Chem.*, 2017, **1**, 0071.
18 T. Jian, W. L. Li, X. Chen, T. T. Chen, G. V. Lopez, J. Li and L. S. Wang, *Chem. Sci.*, 2016, **7**, 7020–7027.
19 J. Wang, T. Yu, Y. Gao and Z. Wang, *Sci. China. Mater.*, 2017, **60**, 1264–1268.
20 L. S. Wang, *Int. Rev. Phys. Chem.*, 2016, **35**, 69–142.
21 H. J. Zhai, Y. F. Zhao, W. L. Li, Q. Chen, H. Bai, H. S. Hu, Z. A. Piazza, W. J. Tian, H. G. Lu and Y. B. Wu, *Nat. Chem.*, 2014, **6**, 727–731.
22 Q. Chen, W. L. Li, Y. F. Zhao, S. Y. Zhang, H. S. Hu, H. Bai, H. R. Li, W. J. Tian, H. G. Lu and H. J. Zhai, *ACS Nano.*, 2015, **9**, 754–760.
23 Y. J. Wang, Y. F. Zhao, W. L. Li, T. Jian, Q. Chen, X. R. You, T. Ou, X. Y. Zhao, H. J. Zhai and S. D. Li, *J. Chem. Phys*, 2016, **144**, 064307.
24 H. J. Zhai, S. D. Li and L. S. Wang, *J. Am. Chem. Soc.*, 2007, **129**, 9254–9255.
25 B. I. Loukhovitski, A. V. Pelevkin and A. S. Sharipov, *Phys. Chem. Chem. Phys.*, 2022, **24**, 13130–13148.
26 S. D. Li, H. J. Zhai and L. S. Wang, *J. Am. Chem. Soc.*, 2008, **130**, 2573–2579.
27 D. Z. Li, L. Y. Feng, L. J. Zhang, L. Pei, W. J. Tian, P. F. Li and H. J. Zhai, *J. Phys. Chem. A*, 2018, **122**, 2297–2306.
28 T. B. Tai, M. T. Nguyen and D. A. Dixon, *J. Phys. Chem. A*, 2010, **114**, 2893–2912.
29 S. J. Gao, P. F. Han, J. C. Guo and H. J. Zhai, *J. Mol. Struct.*, 2024, **1295**, 136769.
30 T. B. Tai and M. T. Nguyen, *Chem. Phys. Lett.*, 2009, **483**, 35–42.
31 W. J. Tian, X. R. You, D. Z. Li, T. Ou, Q. Chen, H. J. Zhai and S. D. Li, *J. Chem. Phys*, 2015, **143**, 064303.
32 W. J. Tian, Z. Y. Guo and M. Yan, *J. Chem. Phys*, 2024, **161**, 084301.
33 S. J. Gao, J. C. Guo and H. J. Zhai, *Front. Chem.*, 2022, **10**, 868782.
34 M. L. Drummond, V. Meunier and B. G. Sumpter, *J. Phys. Chem. A*, 2007, **111**, 6539–6551.
35 M. T. Nguyen, M. H. Matus, V. T. Ngan, D. J. Grant and D. A. Dixon, *J. Phys. Chem. A*, 2009, **113**, 4895–4909.
36 H. J. Zhai, Q. Chen, H. Bai, S. D. Li and L. S. Wang, *Acc. Chem. Res.*, 2014, **47**, 2435–2445.
37 B. M. Gimarc and N. Trinajstic, *Inorg. Chem.*, 1982, **21**, 21–25.
38 W. Z. Yao, J. C. Guo, H. G. Lu and S. D. Li, *Int. J. Quantum Chem.*, 2010, **110**, 2689–2696.
39 X. Y. Tang, Z. H. Cui, C. B. Shao and Y. H. Ding, *Int. J. Quantum Chem.*, 2012, **112**, 1299–1306.
40 D. Z. Li, R. Li, L. J. Zhang, T. Ou and H. J. Zhai, *Phys. Chem. Chem. Phys.*, 2016, **18**, 21412–21420.
41 D. Z. Li, S. G. Zhang and C. C. Dong, *Chem. – Eur. J.*, 2016, **2016**, 1103–1107.
42 L. J. Zhang, L. Y. Feng, H. Bian, L. Pei, D. Z. Li and H. J. Zhai, *Int. J. Quantum Chem.*, 2020, **120**, e26229.
43 S. P. Kuntar, A. Ghosh and T. K. Ghanty, *J. Phys. Chem. A*, 2022, **126**, 7888–7900.
44 A. Sommer, P. N. Walsh and D. White, *J. Chem. Phys*, 1960, **33**, 296.
45 F. T. Greene and P. W. Gilles, *J. Am. Chem. Soc.*, 1962, **84**, 3598–3599.
46 H. Y. Chen and P. W. Gilles, *J. Am. Chem. Soc.*, 1970, **92**, 2309–2312.
47 F. T. Greene and P. W. Gilles, *J. Am. Chem. Soc.*, 1964, **86**, 3964–3969.
48 H. Y. Chen and P. W. Gilles, *J. Phys. Chem.*, 1972, **76**, 2035–2038.
49 D. Z. Li, H. Bai, T. Ou, Q. Chen, H. J. Zhai and S. D. Li, *J. Chem. Phys*, 2015, **142**, 014302.
50 L. J. Zhao, X. L. Xu, H. G. Xu, G. Feng and W. J. Zheng, *New J. Chem.*, 2018, **42**, 16021–16026.
51 S. X. Li, Y. J. Yang and D. L. Chen, *ACS Omega*, 2023, **8**, 30757–30767.
52 W. D. Lu, D. Wang, Z. Zhao, W. Song, W. C. Li and A. H. Lu, *ACS Catal.*, 2019, **9**, 8263–8270.
53 R. W. Dorn, L. O. Mark, I. Hung, M. C. Cendejas, Y. Xu, P. L. Gor'kov, W. Mao, F. Ibrahim, Z. Gan and I. Hermans, *J. Am. Chem. Soc.*, 2022, **144**, 18766–18771.
54 P. Han, R. Yan, Y. Wei, L. Li, J. Luo, Y. Pan, B. Wang, J. Lin, S. Wan and H. Xiong, *J. Am. Chem. Soc.*, 2023, **145**, 10564–10575.
55 J. Tian, G. Collinge, S. F. Yuk, J. Lin, V. A. Glezakou, M. S. Lee, Y. Wang and R. Rousseau, *ACS Catal.*, 2023, **13**, 8219–8236.
56 J. Tian, J. Tan, Z. Zhang, P. Han, M. Yin, S. Wan, J. Lin, S. Wang and Y. Wang, *Nat. Commun.*, 2020, **11**, 5693.
57 H. Yan, S. Alayoglu, W. Wu, Y. Zhang, E. Weitz, P. C. Stair and J. M. Notestein, *ACS Catal.*, 2021, **11**, 9370–9376.
58 L. Li and L. Cheng, *J. Chem. Phys*, 2013, **138**, 094312.
59 J. Guan, X. Zhang, Q. Li, K. Deng, P. Jena and E. Kan, *Nanoscale*, 2021, **13**, 3627–3632.
60 X. Li, B. Cui, W. Zhao, Y. Xu, D. Zou and C. Yang, *Nanotechnology*, 2021, **32**, 225401.
61 L. Li, X. Chen, Y. Huang, P. Zhang, D. Zhou, G. Zhang and B. Xiao, *Appl. Surf. Sci.*, 2022, **602**, 154295.
62 J. Zhang and M. Dolg, *Phys. Chem. Chem. Phys.*, 2015, **17**, 24173–24181.
63 J. Zhang and M. Dolg, *Phys. Chem. Chem. Phys.*, 2016, **18**, 3003–3010.
64 J. P. Doye and D. J. Wales, *Phys. Rev. Lett.*, 1998, **80**, 1357.
65 S. Kirkpatrick, C. D. Gelatt Jr and M. P. Vecchi, *Science*, 1983, **220**, 671–680.
66 J. J. Stewart, *J. Mol. Model.*, 2007, **13**, 1173–1213.
67 C. Bannwarth, S. Ehlert and S. Grimme, *J. Chem. Theory Comput.*, 2019, **15**, 1652–1671.

68 S. Grimme, J. Antony, S. Ehrlich and H. Krieg, *J. Chem. Phys*, 2010, **132**, 154104.
69 Y. Zhao and D. G. Truhlar, *Theor. Chem. Acc.*, 2008, **120**, 215–241.
70 P. C. Hariharan and J. A. Pople, *Theor. Chim. Acta.*, 1973, **28**, 213–222.
71 W. J. Hehre, R. Ditchfield and J. A. Pople, *J. Chem. Phys*, 1972, **56**, 2257–2261.
72 M. J. Frisch, G. W. Trucks, H. B. Schlegel, G. E. Scuseria, M. A. Robb, J. R. Cheeseman, G. Scalmani, V. Barone, B. Mennucci, G. A. Petersson, H. Nakatsuji, M. Caricato, X. Li, H. P. Hratchian, A. F. Izmaylov, J. Bloino, G. Zheng, J. L. Sonnenberg, M. Hada, M. Ehara, K. Toyota, R. Fukuda, J. Hasegawa, M. Ishida, T. Nakajima, Y. Honda, O. Kitao, H. Nakai, T. Vreven, J. A. J. Montgomery, J. E. Peralta, F. Ogliaro, M. Bearpark, J. J. Heyd, E. Brothers, K. N. Kudin, V. N. Staroverov, R. Kobayashi, J. Normand, K. Raghavachari, A. Rendell, J. C. Burant, S. S. Iyengar, J. Tomasi, M. Cossi, N. Rega, N. J. Millam, M. Klene, J. E. Knox, J. B. Cross, V. Bakken, C. Adamo, J. Jaramillo, R. Gomperts, R. E. Stratmann, O. Yazyev, A. J. Austin, R. Cammi, C. Pomelli, J. W. Ochterski, R. L. Martin, K. Morokuma, V. G. Zakrzewski, G. A. Voth, P. Salvador, J. J. Dannenberg, S. Dapprich, A. D. Daniels, O. Farkas, J. B. Foresman, J. V. Ortiz, J. Cioslowski and D. J. Fox, *Gaussian 16, Revision A.03*, Wallingford CT, 2016, vol. 2016.
73 B. Chan, J. Deng and L. Radom, *J. Chem. Theory Comput.*, 2011, **7**, 112–120.
74 K. B. Wiberg, *Tetrahedron*, 1968, **24**, 1083–1096.
75 D. Y. Zubarev and A. I. Boldyrev, *Phys. Chem. Chem. Phys.*, 2008, **10**, 5207–5217.
76 T. Lu and F. Chen, *J. Comput. Chem.*, 2012, **33**, 580–592.
77 C. Legault, *CYLview20*, 2020, **https://www.cylview.org**.
78 G. Knizia, *J. Chem. Theory Comput.*, 2013, **9**, 4834–4843.
79 W. Humphrey, A. Dalke and K. Schulten, *J. Mol. Graphics*, 1996, **14**, 33–38.
80 E. Francisco, A. Martín Pendás, M. García-Revilla and R. Álvarez Boto, *Comput. Theor. Chem*, 2013, **1003**, 71–78.
81 M. Menéndez, R. Álvarez Boto, E. Francisco and A. Martín Pendás, *J. Comput. Chem.*, 2015, **36**, 833–843.
82 E. V. Bukovsky, A. M. Pluntze and S. H. Strauss, *J. Fluorine. Chem.*, 2017, **203**, 90–98.
83 J. C. Axtell, L. M. Saleh, E. A. Qian, A. I. Wixtrom and A. M. Spokoyny, *Inorg. Chem.*, 2018, **57**, 2333–2350.
84 K. R. Asmis, B. B. Beele, C. Jenne, S. Kawa, H. Knorke, M. C. Nierstenhöfer, X. B. Wang, J. Warneke, Z. Warneke and Q. Yuan, *Chem. – Eur. J.*, 2020, **26**, 14594–14601.
85 M. E. Kilic and P. J. Jena, *Phys. Chem. Lett.*, 2023, **14**, 8697–8701.
86 M. E. Kilic and P. J. Jena, *Phys. Chem. A*, 2024, **128**, 1993–2002.
87 B. Miao, Z. Qiu, Z. Zhen, Y. Yang, Z. Yang, T. Xiao, J. Lv, S. Huang, Y. Wang and X. Ma, *Phys. Chem. Chem. Phys.*, 2024, **26**, 10494–10505.
88 M. M. Shmakov, S. A. Prikhod'ko, V. N. Panchenko, M. N. Timofeeva, V. V. Bardin, V. N. Parmon and N. Y. Adonin, *Catal. Rev.*, 2024, 1–47.